Intravitreous Delivery of the Corticosteroid Fluocinolone Acetonide Attenuates Retinal Degeneration in S334ter-4 Rats

Inna V. Glybina,[1] Alexander Kennedy,[1] Paul Ashton,[2] Gary W. Abrams,[1] and Raymond Iezzi[1,3]

Purpose. To study the neuroprotective properties of low-dose, sustained-release intravitreous fluocinolone acetonide (FA) in transgenic S334ter-4 rats.

Methods. S334ter-4 rats aged 4 weeks were divided into four groups: 0.5 μg/d FA-loaded intravitreous drug delivery implant (IDDI); 0.2 μg/d FA-loaded IDDI; inactive IDDI; and unoperated controls. Electroretinography (ERG) was performed before surgery and every 2 weeks after surgery for 8 weeks. When the rats were 12 weeks of age, outer nuclear layer (ONL) and inner nuclear layer (INL) thicknesses were measured. Microglial cell counts were obtained from retinal wholemounts labeled for Iba-1.

Results. At the end of the study, unoperated and inactive IDDI-implanted rats demonstrated 50% to 60% reductions in ERG amplitudes compared with those recorded at 4 weeks ($P < 0.001$ for both groups). FA 0.2-μg/d animals demonstrated 15% amplitude attenuation, while FA 0.5-μg/d animals showed 30% reduction. ONL thickness in FA 0.2-μg/d–treated eyes was 25.8% ± 2.3% higher than in control group eyes ($P <$ 0.001) and 30.0% ± 2.1% higher than in inactive IDDI-implanted eyes ($P < 0.001$). In FA 0.5-μg/d–treated eyes, ONL thickness was 22.4% ± 2.8% higher than in control group eyes ($P < 0.001$) and 22.3% ± 3.7% higher than in inactive IDDI-implanted eyes ($P < 0.01$). No statistically significant difference was observed between the two control groups. No statistically significant difference between the two FA-treated groups was found. FA-treated groups demonstrated significantly fewer activated microglial cells than control groups.

Conclusions. Chronic intravitreous infusion of FA preserves ONL cell morphology and ERG a- and b-wave amplitudes and reduces retinal neuroinflammation in S334ter rats. Based on these findings, the synthetic corticosteroid FA may promise a therapeutic role in patients with retinal degeneration. (*Invest Ophthalmol Vis Sci.* 2010;51:4243–4252) DOI:10.1167/iovs.09-4492

Retinitis pigmentosa (RP) is a group of autosomal recessive, autosomal dominant, and X-linked diseases resulting in photoreceptor cell death, severe visual impairment, or blindness. Although many of the genetic, biochemical, and phenotypic changes occurring in RP are well understood, no therapy exists to treat any of the known pathophysiological mechanisms. In this article, we will discuss the role of neuroinflammation in the progression of retinal neurodegeneration and possible treatment strategies for targeting the immunologic aspects of RP.

Microglia, the major immunocompetent cells of the central nervous system (CNS), represent an acutely responsive, tissue-based system providing maintenance of extracellular ionic homeostasis,[1,2] scavenging of viruses, bacteria, dead neurons, and any cell debris,[1–4] and neural cell repair.[1,2,5] A large number of studies have shown that microglial cells are responsible for neuroinflammation associated with several neurodegenerative diseases of the CNS and may contribute to the progression of neuronal cell death.[1,6–11] The origin of microglia remains a subject of investigation. One major hypothesis suggests that microglial cells derive from a line of monocyte/macrophage cells that enter the CNS from the blood circulation during embryonic development and the early postnatal period and, on arrival to the designated tissue sites, differentiate into resident microglia.[12–14] The origin of retinal microglia is still poorly understood, though they are suspected to have an origin similar to that of CNS microglia. One study performed on animal embryos showed that macrophages invade the retina from the cephalic mesenchyme and then transform into microglia.[15] Two other studies in quail embryo eyes[16,17] showed that ameboid macrophages, which transform into microglia, enter the retina from two sites: the optic nerve, where they populate retina moving from the center to the periphery and from the inner to the outer retina by migrating on the endfeet of Müller cells, creating layers at the levels of ganglion cells, inner plexiform layer, and outer plexiform layer; and the ciliary body, where they are suspected to have an origin similar to that of ciliary body dendritic cells. Similar pools of microglia were described in human fetal retinas.[18]

Microglial cells have a ramified morphology with a small cell body and multiple lengthy dendritic processes. Resting microglia have low expression of membrane receptors; however, they quickly transform into phagocytes when stimulated by infectious agents, cellular debris, and membrane fragments, such as lipopolysaccharides.[1,2,6,19] Within 24 hours of activation, microglial cells enlarge, acquire an ameboid macrophage-like shape, and react by upregulating IgG, CD1 receptor, and intercellular adhesion molecules.[20] They also release cytotoxic molecules, including tumor necrosis factor (TNF)-α, IL-1β, IL-

10, IFN-γ, hydrogen peroxide, and superoxide anion.[3,20–23] When the activating stimulus is eliminated, microglia quickly return to their resting state.[2] However, when the stimulus continues, microglial cells express major histocompatibility complex (MHC) class I and II molecules[3,4] and inflammatory glycoproteins,[24] which are self-stimulating and stimulate/recruit other immune cells. Microglia then cluster around neurons, adhere to their surfaces, constitutively produce cytotoxins that lead to neuronal death, and consequently recruit and activate additional microglia.[1,21,25]

A large body of evidence from CNS studies of microglial activation and neurotoxicity in neural degeneration has led to research into the pathogenicity of retinal microglia. Studies of retinal dystrophic rodents have demonstrated similar findings: outer retinal degenerations are associated with significant microglial activation and microgliosis within the outer retina.[26–28] Sphingolipids within damaged photoreceptor cell membranes activate microglial cells, inducing them to express chemoattractants that stimulate migration of the microglial cells toward the ONL.[29] Retinal microglia, in turn, express cytotoxic molecules and growth factors, killing photoreceptor cells by apoptosis and necrosis.[29–31] Large accumulations of activated photoreceptor-containing microglia have been described within the outer retinas of cadaveric human eyes with RP, late-onset retinal degeneration, and age-related macular degeneration.[32]

In our previous study of Royal College of Surgeons (RCS) rats,[33] we demonstrated two principal phenomena. First, retinal degeneration in RCS rats is accompanied by massive migration of activated microglia toward the outer retina and the debris zone, which forms between the retinal pigment epithelium (RPE) and photoreceptors. This observation agrees with earlier studies.[27,34] Second, chronic intravitreous delivery of low-dose fluocinolone acetonide (FA) is associated with profound suppression of this microglial response, significant preservation of photoreceptors, and electroretinograms. FA is a synthetic corticosteroid, FDA-approved for sustained-release intravitreous delivery. The FA-loaded drug delivery device used in the present study and our previous study in RCS rats is similar to (but smaller than) the FDA-approved device for the treatment of patients with severe noninfectious posterior uveitis.[35–37] In this study, we used the heterozygote S334ter-4 rat retinal degeneration model, which is highly similar to a human rhodopsin mutation in RP. RCS rat and S334ter rat retinal degenerations, though referred to as RP entities, have different underlying mechanisms. RCS rats have a frameshift mutation in the Mertk gene encoding tyrosine kinase receptor[38,39] that results in impaired phagocytosis of shed photoreceptor outer segments by the RPE and thus rapid photoreceptor cell death. Transgenic S334ter-4 rats develop slow photoreceptor cell death because of a mutant rhodopsin gene terminating at residue 334. In RCS rats, accumulation of peroxidized lipid membranes causes the formation of a thick subretinal debris layer that stimulates microglial cells to assume a phagocytic phenotype and migrate to the outer retina to scavenge the debris. S334ter rats do not produce a debris layer that directly stimulates microglia. Thus, the purpose of the present study was to determine the existence, intensity, and distribution of retinal neuroinflammation in S334ter-4 rats and whether the neuroprotective properties of FA we observed in RCS rats apply to the S334ter primary rhodopsin mutation model of RP.

In this study, we investigated microglial activation and distribution and evaluated retinal morphology and function, with and without chronic intravitreous administration of the synthetic corticosteroid, FA, in the transgenic S334ter-4 rat.

METHODS

Animals

Thirty-two S334ter-4 rats were divided into the following experimental groups: FA-loaded intravitreal drug delivery implants (IDDIs) with release rates of 0.5 μg/d, FA-loaded IDDIs with release rates of 0.2 μg/d, inactive IDDIs, and unoperated controls. Littermates were distributed evenly among the experimental groups. Animals received implantation of IDDI at 4 weeks of age. Unoperated controls received the same amount of anesthesia and surgical microscope light exposure as operated animals at the same age. Rats were followed with an anterior segment examination and funduscopy, using an operating microscope (OPMC; Thornwood, NY), intraocular pressure measurements (Tono-Pen XL; Reichert Ophthalmic Instruments, Depew, NY), and ERG testing. These evaluations were performed immediately before the IDDI implantation surgery and every 2 weeks after surgery for 8 weeks. There was a total of five ERG sessions. Animals were killed on the day of the last ERG. Thicknesses of the retinal outer and inner nuclear layers were measured from histologic retinal sections using the eyes of five animals from each experimental group. Immunohistochemical analysis of retinal microglia was performed on the eyes of the remaining three rats from each group. Rats were maintained and treated in accordance with the ARVO Statement for the Use of Animals in Ophthalmic and Vision Research.

Surgery

All implantations were performed on the right eye using an operating microscope (OPMC; Zeiss). Surgery was conducted under sterile conditions and general anesthesia using intraperitoneal injection of ketamine (67 mg/kg) and xylazine (10 mg/kg). The area around the eye was treated with 10% povidone iodine and 70% ethanol solutions. The anesthetized animal was then positioned on a heating pad for the entire procedure to maintain core body temperature. IDDIs are 2-mm-long cylinders with diameters of 300 μm (Fig. 1). Both the injectors and the implants for intravitreous implantation were provided by pSivida Corp. (Watertown, MA). Implants were inserted into the vitreous cavity transsclerally, through the pars plana in the superior-temporal quadrant, using a specially designed injector. The transscleral perforation was closed with a 50-μm-thick cyanoacrylate bioadhesive-fixed polyimide patch. The conjunctiva was positioned over the patch and fixed with the same adhesive. At the end of the procedure, intramuscular injection of butorphanol 0.1 mg/kg was given for pain prevention.

Electrophysiology

ERG testing was performed under general anesthesia with intraperitoneal injection of ketamine (67 mg/kg) and xylazine (10 mg/kg), after
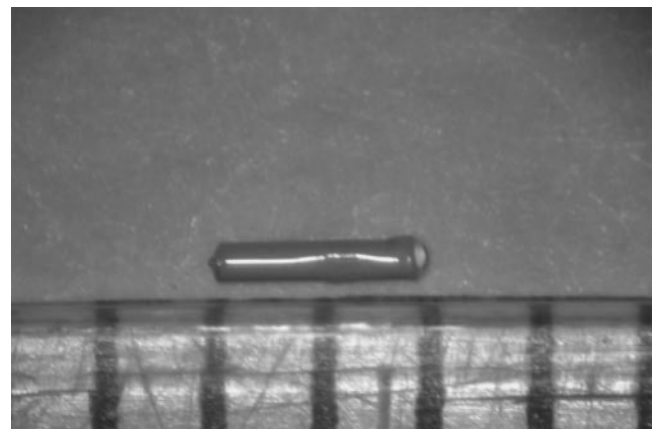

FIGURE 1. Intravitreal drug delivery implant placed next to a ruler with 1-mm divisions.

12-hour overnight dark adaptation. Pupils were dilated with topical 1% tropicamide and 2.5% phenylephrine solutions. To prevent corneal dehydration, 0.9% saline was periodically applied to the corneas during the ERG session. ERG responses were recorded from both eyes simultaneously using platinum wire loop corneal electrodes mounted to the surface of white clear light-emitting diodes (CMD204; UWC, series T-1; Innovative Technologies Inc., Chantilly, VA), with a flash intensity of 25 cd · s/m². Platinum needle reference electrodes were placed through the ears. The abdomen of the animal was shaved and positioned on a conductive gel over grounded aluminum foil. Fifteen 1-ms flashes were delivered to both eyes simultaneously with the interstimulus interval of 10 seconds. The signals were bandpass filtered at 10 to 100 Hz.

ERG Data Analysis

After artifact rejection, ERG waveforms were averaged for each eye over 15 traces at each recording session. The a-wave amplitude was defined as the amplitude of the negative slope preceding the leading positive slope. The b-wave amplitude was defined as the peak-to-peak amplitude of the leading positive slope (from the lowest point of the a-wave to the highest point of the b-wave). The implicit times of the a- and b-waves were measured, defined as timing of the most negative point (a-wave peak) and the most positive point (b-wave peak). These were measured from each of the averaged ERG waveforms. Individual and group means and standard deviations of all ERG parameters were computed for right and left eyes at each time point. One-way ANOVA was performed for the 8-week postoperative ERG data. Comparisons of initial ERG to the end point ERG parameters within each group were performed using paired *t*-tests when appropriate.

Histology

Enucleated eyes were immersed in Karnofsky fixative overnight, at 4°C, rinsed with 0.01 M phosphate-buffered solution, dehydrated in serial dilutions of alcohol, cleared with xylene substitute (Pro-Par; Anatech Ltd., Battle Creek, MI), and embedded in paraffin containing DMSO (Fisher Scientific, Pittsburgh, PA). Transverse 6-μm-thick whole-eye paraffin sections were mounted on poly-L-lysine–coated glass slides and stained using Harris hematoxylin and eosin.

Retinal Histology Analysis

To evaluate the degree of retinal degeneration, outer nuclear layer (ONL) and inner nuclear layer (INL) thicknesses were measured using the method of LaVail.[40-42] For each experimental eye, ONL and INL thickness measurements were taken from three entire retinal sections. Measurements were made using an eyepiece with a micrometer scale over a 330-μm diameter microscopic field (Zeiss, Oberkochen, Germany). Within each field, three measurements of both the ONL and the INL thicknesses were taken: the first measurement was taken in the center of the field, and the other two measurements were taken 100 μm away from the center on each side. Thus, in each retinal section, 20 sets of three ONL measurements and three INL measurements were obtained. The first set of measurements was always taken one microscopic field away from the optic nerve head (approximately 330 μm), and subsequent sets were taken toward the periphery. For each group, mean ONL and INL thickness measurements for all retinal eccentricities were computed for further statistical comparison. To demonstrate the distribution of the ONL thicknesses across the retina within groups, measurements were plotted as a function of eccentricity. One-way ANOVA was performed for the ONL and INL thicknesses among all groups.

Immunohistochemistry

Enucleated eyes were kept in buffered 10% formalin for 4 hours at 4°C and were processed as retinal wholemounts.

Microglia Staining in Wholemounted Retina

To stain both resting and activated microglial cells within the retinal wholemounts, three primary antibodies were used. Total microglial cell counts were made using the microglial marker ionized calcium-binding adapter molecule (Iba)-1 antibody (Wako Chemicals USA Inc., Richmond, VA).[43] To determine the presence of microglia expressing phagocytic activity, an antibody to the lysosomal membrane protein ED-1 (Serotec Ltd., Oxford, UK)[44] was used. We used ED-2 (a protein in monocytes and most macrophages) antibody (Serotec Ltd.), as a marker of infiltrating macrophages.[44] Goat anti-rabbit TRITC-conjugated antibody for Iba-1 and goat anti-mouse FITC-conjugated antibody for ED-1 (Sigma-Aldrich, St. Louis, MO) were used as secondary antibodies. After fixation, retinas were carefully removed and placed in PBS containing 1% Triton X-100 for 1 hour at room temperature. Before staining, retinas were blocked with 5% normal goat serum and then incubated overnight at 4°C in a cocktail of Iba-1 antibody at 1:200 dilution and ED-1 antibody at 1:100 dilution in PBS containing 0.1% Triton X-100. After several washes, retinas were incubated in the secondary antibody solution for 4 hours at room temperature, washed again, mounted inner limiting membrane (ILM)-side down on glass slides, and coverslipped with mounting medium (Vectashield; Vector Laboratories, Burlingame, CA).

Microglial Cell Count Analysis

An epifluorescence microscope (B-MAX 50; Olympus America, Melville, NY) was used for microglial cell counts.

Nasal hemiretinae were used for microglial cell counting. In the retinal wholemount preparations, Iba-1 antibody-labeled microglial cell counts were made in six standardized fields at defined levels within the retina. Starting 200 μm from the edge of the optic nerve, three nonoverlapping superior nasal and three inferior nasal 400× microscopic fields were selected, spaced approximately 100 μm apart, top to bottom, and centered approximately 200 μm from the sagittal hemiretinal incision edge. Microglial cell layers within the whole-mounted retina were localized using confocal microscopy (Axiophot Triple-Camera Photomicroscope with an Apotome module; Carl Zeiss). Four layers of microglial cell bodies were defined at the levels of the ILM, ganglion cells, bipolar cell layer (INL), and retinal photoreceptors (ONL). Means and standard deviations were computed for total microglial cell counts for each layer among all eyes in each group. One way ANOVA was performed for the microglial cell counts among all groups.

RESULTS

No signs of infection, inflammation, media opacities, or ocular hypertension were observed during the 8-week postoperative period in any animal.

Electroretinography

ERG of the FA-treated eyes showed moderate amplitude reduction and virtually no implicit time delays throughout the study course, though IDDI-treated eyes and unoperated eyes showed substantial depressions of the ERG amplitudes at every recording session, along with gradual prolongation of the implicit times. Figure 2 shows mean ERG traces for each experimental group across the study course.

ERG a-Wave

Figures 3A and 3B illustrate ERG a-wave amplitudes across the study in all groups. In unoperated control eyes, a-wave amplitudes dropped rapidly between 4 and 8 weeks of age (over 50% amplitude loss), compared with the initial ERGs in this group. Amplitude reduction rates then slowed and by the end of the study were 63.2% ± 9.4% less than the initial values ($P <$ 0.001). A similar pattern was observed in the inactive IDDI-treated eyes, whose end point amplitudes were 58.7% ± 8.0%
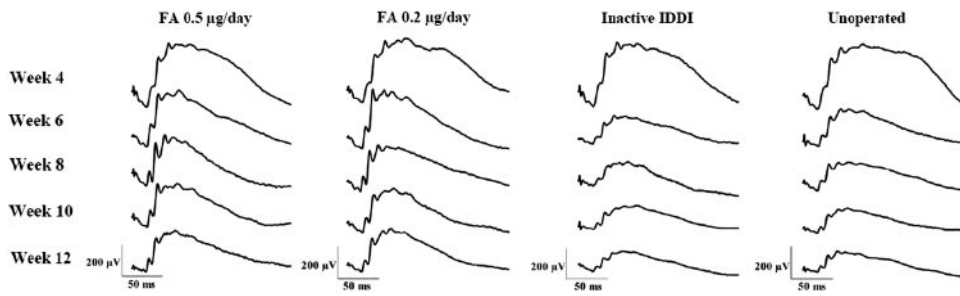
FIGURE 2. Representative ERG traces among four experimental groups of S334ter-4 rats throughout the study course. Week designations correspond to animals' ages.

lower than their initial values ($P < 0.001$). No statistically significant difference was found in the end point values between these two groups ($P > 0.59$). ERG a-wave amplitude loss was significantly lower in both FA-treated groups, with better preservation seen in the eyes treated with the lower daily FA dose. End point a-wave amplitudes in the FA 0.2-µg/d–treated eyes were 22.3% ± 15.5% lower than initial ERGs; the difference was not statistically significant ($P = 0.09$). In the FA 0.5-µg/d–treated eyes, end point a-wave amplitudes showed 37.7% ± 10.7% reduction compared with the initial ERGs, which appeared to be significant ($P = 0.029$). There was no statistically significant difference in end point ERG a-wave amplitudes between the two FA groups ($P > 0.1$). End point a-wave amplitudes were significantly greater in the FA 0.2-µg/ d–treated eyes compared with the unoperated control eyes ($P < 0.001$) and with the inactive IDDI-treated eyes ($P < 0.01$). However, end point a-wave amplitudes of the FA 0.5-µg/d– treated eyes were significantly greater only compared with the unoperated control eyes ($P < 0.05$) and did not show statistically significant differences compared with the inactive IDDI-treated eyes ($P = 0.118$). In addition, left (unoperated) eyes of the FA 0.2-µg/d–treated animals also showed significant preservation of the ERG a-wave amplitudes compared with both control groups ($P < 0.05$). ERG a-wave implicit times (Figs. 4A, 4B) did not show statistically significant changes during the study within or between groups.

ERG b-Wave

Figures 3C and 3D show ERG b-wave amplitudes during the study in all groups. As in the case of a-waves, the most dramatic reduction of the b-wave amplitudes (approximately 50%) in the two control groups occurred during the first month of the experiment. Reduction rates slowed during the second month of the study. Compared with the initial b-waves, the end point b-waves showed 58.9% ± 10.4% amplitude losses in the unoperated control eyes ($P < 0.00001$) and 69.6% ± 2.2% amplitude losses in the inactive IDDI-treated eyes ($P < 0.00001$). In the FA 0.2-µg/d–treated eyes, end point b-wave amplitudes showed 29.6% ± 6.8% reductions compared with the initial ERGs, achieving statistical significance ($P < 0.01$); in the FA 0.5-µg/d–treated eyes, the end point ERG b-wave amplitudes showed 43.1% ± 5.7% reductions, compared with the initial ERGs, which were also significant ($P < 0.01$). End point ERG b-wave amplitudes were significantly greater in the FA 0.2-µg/ d–treated eyes than in the unoperated control eyes ($P < 0.0001$) or the inactive IDDI-treated eyes ($P < 0.0001$). They were also significantly greater in the FA 0.5-µg/d–treated eyes than in the unoperated control eyes ($P < 0.05$) or the inactive IDDI-treated eyes ($P < 0.01$). There was no statistically significant difference between the two FA-treated groups ($P = 0.1$), nor were there statistically significant differences between the two control groups ($P > 0.18$).

ERG b-wave implicit times (Figs. 4C, 4D) did not change significantly within either FA treatment group during the study (initial vs. end point); however, in the unoperated control eyes, the end point ERG b-waves were delayed by 16.2% ± 6.2% compared with the initial ERGs. In the inactive IDDI-treated eyes, end point ERG b-waves were delayed by 10.9% ± 6.6% compared with the initial ERGs, both of which appeared significantly greater than the end point ERG b-wave implicit
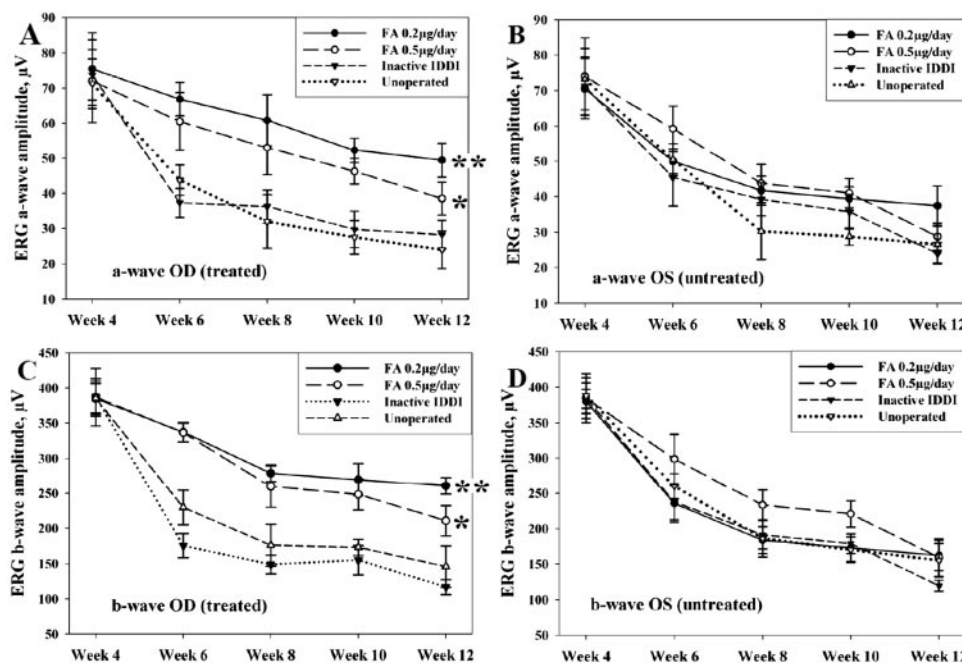

FIGURE 3. Mean (±SE) ERG a-wave and b-wave amplitudes in treated (OD) and untreated (OS) eyes of S334ter-4 rats throughout the study course among four experimental groups. (A) ERG a-wave amplitudes for the right (OD, treated) eyes. (B) ERG a-wave amplitudes for the left (OS, untreated) eyes. (C) ERG b-wave amplitudes for the right (OD, treated) eyes. (D) ERG b-wave amplitudes for the left (OS, untreated) eyes. (A) *$P < 0.05$; **$P < 0.001$. (C) *$P < 0.01$; **$P < 0.0001$, compared with both inactive IDDI-treated and unoperated control eyes for the end time point ERG measurements. Week designations correspond to animals' ages.
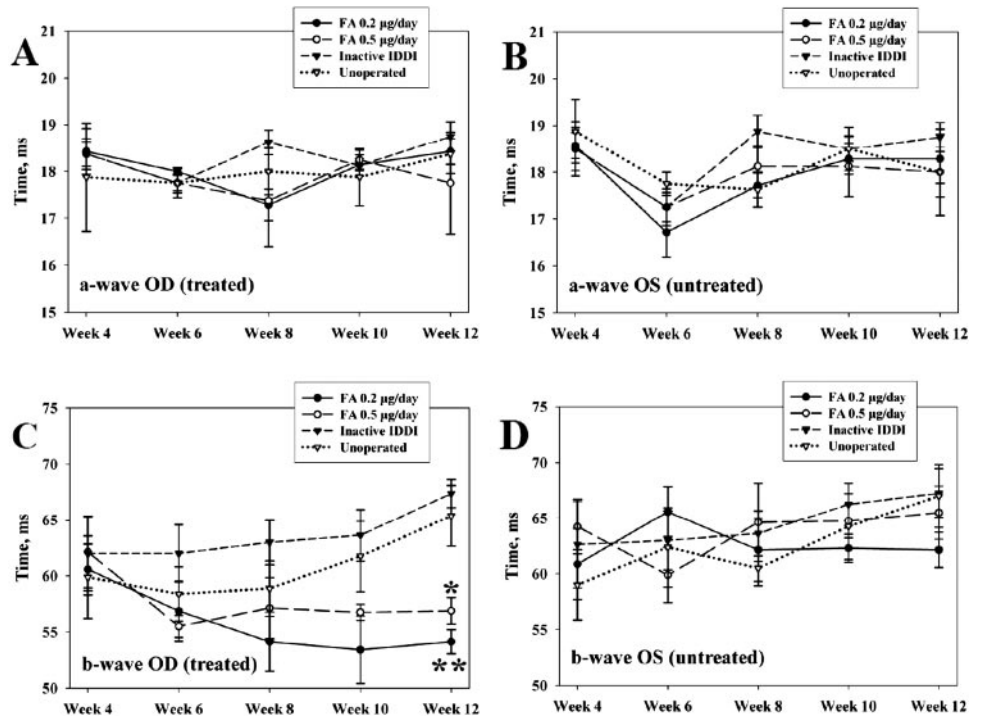
FIGURE 4. Mean (±SE) ERG a-wave and b-wave implicit times in treated (OD) and untreated (OS) eyes of S334ter-4 rats throughout the study course among four experimental groups. (**A**) ERG a-wave implicit times for the right (OD, treated) eyes. (**B**) ERG a-wave implicit times for the left (OS, untreated) eyes. (**C**) ERG b-wave implicit times for the right (OD, treated) eyes. (**D**) ERG b-wave implicit times for the left (OS, untreated) eyes. (**C**) *$P < 0.001$; **$P < 0.0001$, compared with both inactive IDDI-treated and unoperated control eyes for the end time point ERG measurements. Week designations correspond to animals' ages.

times in the FA 0.2-μg/d–treated eyes ($P < 0.0001$) and in the FA 0.5-μg/d-treated eyes ($P < 0.001$).

Histology

Representative photomicrographs of retinal histology are shown in Figure 5. Mean ONL and INL thicknesses for right (treated) eyes of each group are summarized in Figure 6. Mean ONL thickness distribution throughout the retina is diagrammed in Figure 7. ONLs of the eyes from unoperated control and inactive IDDI eyes showed areas of three to four,

sometimes five, cell rows. ONL thicknesses were not statistically different between these two groups ($P = 0.6$). FA 0.2-μg/d eyes demonstrated ONLs containing six to eight rows of photoreceptor cells; the ONL was significantly thicker than in unoperated control eyes ($P < 0.00001$) and eyes that received inactive IDDIs ($P < 0.00001$). Eyes implanted with FA 0.5 μg/d showed five to six, occasionally four or seven, ONL cell rows; the ONL was significantly thicker than in unoperated controls ($P < 0.01$) or in the inactive IDDI eyes ($P < 0.05$). The ONL of the FA 0.2 μg/d eyes appeared significantly thicker than in the
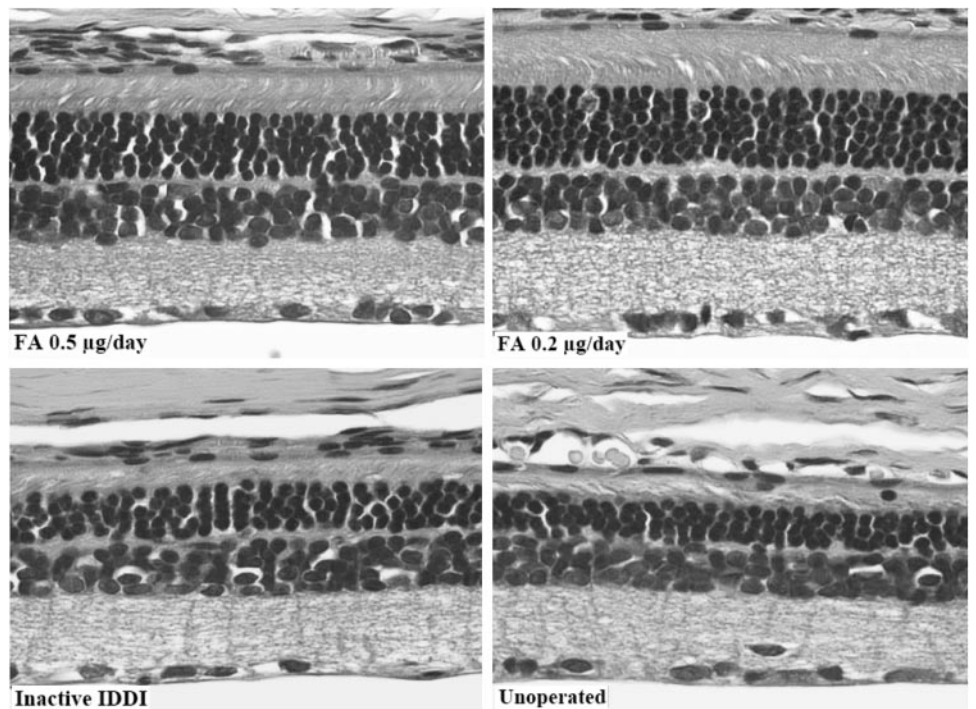

FIGURE 5. Micrographs (200×) of representative retinal histologic sections (hematoxylin and eosin staining) among four experimental groups of 12-week S334ter-4 rats.
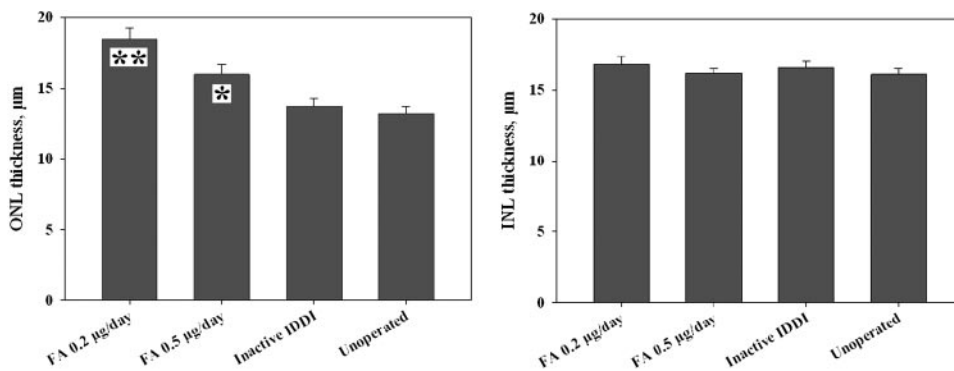
FIGURE 6. Mean (±SE) retinal ONL and INL thicknesses among four experimental groups of 12-week S334ter-4 rats. $*P < 0.01$; $**P < 0.00001$, compared with both inactive IDDI-treated and unoperated control eyes.

FA 0.5 μg/d eyes ($P < 0.01$). In addition, the ONL of left (untreated) eyes of the FA 0.2-μg/d group did not significantly differ from that of the FA 0.5-μg/d group and was significantly thicker than in both control groups ($P < 0.01$). INL thickness was not significantly different between groups ($P > 0.6$).

Microglial Cells in Retinal Wholemounts

Figure 8 shows immunofluorescence micrographs of Iba-1–stained microglial cells in the retinal wholemounts, within four layers, among all experimental groups. Figure 9 shows microglial cell counts. Resting microglial cells with ramified morphology were predominant within the ganglion and bipolar cell layers in all groups and did not show significant quantitative differences between the groups. Activated microglial cells with an amoeboid phenotype, with or without one or two thick podia-looking processes, were found predominantly at the ILM level and within the photoreceptor layer and showed striking differences between FA-treated and control eyes. For the ILM layer in the FA 0.2-μg/d eyes, microglial cell counts were 3.9 ± 1.0 times lower than in unoperated control eyes ($P < 0.00001$) and 3.9 ± 0.9 times lower than in inactive IDDI eyes ($P < 0.00001$). Among the FA 0.5-μg/d eyes, microglial cell counts were 4.2 ± 1.1 times lower than in unoperated control eyes ($P < 0.00001$) and 4.3 ± 1.0 times lower than in inactive IDDI eyes ($P < 0.00001$). For the photoreceptor layer, in the FA 0.2-μg/d eyes, microglial cell counts were 8.4 ± 2.5 times lower than in unoperated control eyes ($P < 0.00001$) and 7.6 ± 1.8 times lower than in inactive IDDI eyes ($P < 0.00001$). In FA 0.5-μg/d eyes, microglial cell counts were 5.8 ± 2.4 times lower than in unoperated control eyes ($P < 0.00001$) and 5.5 ± 1.8 times lower than in inactive IDDI eyes

($P < 0.00001$). Microglia counts of left (untreated) eyes of the FA groups did not differ from the control groups. No ED-1– or ED-2–positive cells were found in the retinas of S334ter rats.

DISCUSSION

Our study has shown that chronic intravitreous administration of fluocinolone acetonide, a synthetic corticosteroid, slowed the degeneration of the outer retina and preserved electroretinogram amplitudes in dystrophic S334ter rats. These observations were associated with a profound suppression of retinal neuroinflammation and are consistent with our previous observations in the RCS rat retinal degeneration model.

Rhodopsin gene mutations are prevalent in autosomal dominant RP[45,46] in humans. A high degree of similarity between the transgenic S334ter-4 rat and human RP genotypes and phenotypes makes the S334ter rat a valuable model in examining the pathogenesis of RP and in testing possible treatments. In these rats, photoreceptor cell death is believed to occur by apoptosis associated with failures of mutant rhodopsin sorting and deactivation during phototransduction. This leads to a prolonged ERG response, especially the negative slope of the ERG b-wave, which, in our study, is also clearly seen on the ERG traces (Fig. 2). Photoreceptor cell death starts around postnatal day (P)13 and proceeds at a high rate until approximately P60.[47] It slows to P90 and proceeds at slower rates to almost 1 year of age until the ONL is gone.[47,48] Green et al.[47] demonstrated a correlation between ONL degeneration and severity of mutant rhodopsin missorting within the retina in S334ter-4 rats. They established that at P15, the rhodopsin missorting and misdistribution within the retina is severe and
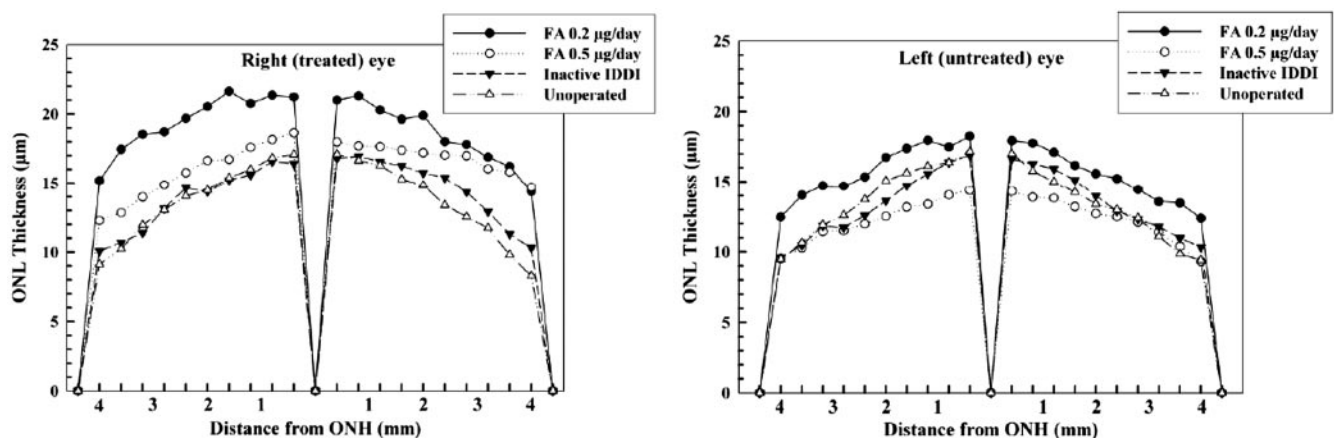

FIGURE 7. Mean measurements of ONL thickness along transverse retinal sections from the optic nerve head to the ora serrata of 12-week S334ter-4 rats among four experimental groups.
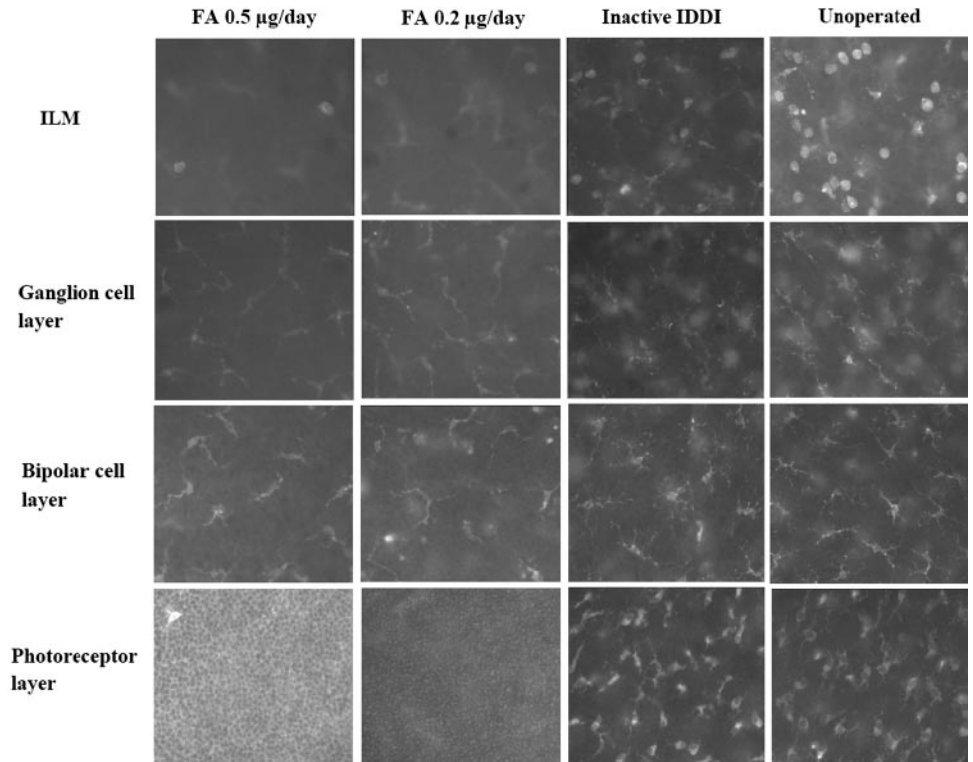
FIGURE 8. Photomicrograph (400×) of Iba-1–labeled microglial cells within different retinal layers of 12-week S334ter-4 rats among four experimental groups.

FIGURE 9. Mean (±SE) Iba-1–labeled microglial cell counts at the level of different retinal layers among four experimental groups of 12-week S334ter-4 rats. *$P < 0.00001$ compared with both inactive IDDI-treated and unoperated control eyes.

that approximately 620,000 photoreceptors are lost per eye per day. By P90, the missorting markedly decreased and was accompanied by loss of 190,000 photoreceptors per eye per day. Our data correlate with these findings in that we observed rapid degradation of ERG in the control rats, within the same time frames. By P56 to P57, their ERG amplitudes were approximately 50% lower than the initial ERGs (obtained at P28). Between P56 and P57 and P84 and P85, rates of the ERG degradation were markedly slower. At P84 to P85 (the end of our study), ONLs of the unoperated and inactive IDDI eyes were 2 to 3.5 times thinner than the normal ONL thickness

(10–12 cell rows[49,50]) of normal rats[49,50] and approximately 1.5 times thinner than those of the FA-treated animals.

We have evaluated treatment effects of two doses of FA: 0.2 μg/d and 0.5 μg/d. Comparison of the initial to final ERGs showed that in the FA 0.2-μg/d–treated eyes, a-wave amplitudes did not change significantly during the study, though significant ERG a-wave loss was observed in the other three groups. The end point ERG b-waves in the FA-treated eyes were significantly greater than those in the control eyes, exceeding them on average by a factor of 2. These observations indicate that steroid treatment was associated with preservation of rod-driven electrical activity during phototransduction. Overall, our findings suggest that steroid FA did not fully prevent S334ter retinal degeneration but significantly suppressed it. We hypothesize that the observed preservation of retinal morphology and electrophysiology in the FA-treated eyes of S334ter rats is associated with the ability of steroid FA to suppress retinal neuroinflammation, which occurs in the RP retina as part of the neurodegenerative process.
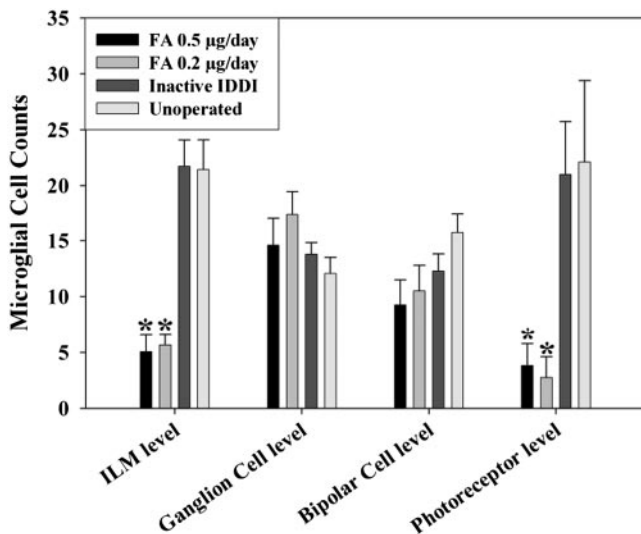
Microglia and Retinal Neurodegeneration

Studies in albino BALB/c mice with photic retinal injury,[26,29] rd-1 mice,[28] RCS rats[27,34] and human RP eyes[32] have demonstrated that accumulation of activated microglia in the degenerative retinas mainly occurred within ONL and the photoreceptor layer and adjacent to the RPE, whereas resident microglia in the absence of retinal degeneration are limited primarily to the inner retina (within bipolar and ganglion cell layers). Ng et al.[26] provided evidence that activated microglia in the outer retina originated from pools of resident microglia in the inner retinal layer. Once activated, retinal microglia release toxic molecules, such as TNF-α and reactive oxygen species, which may induce apoptosis in otherwise healthy cells such as photoreceptors, RPE, and vascular endothelium.[30,31,49]

In our study, we identified four distinct microglial cell layers in S334ter-4 rat retinas. Two of these layers, those at the level of ganglion and bipolar cells, were populated by tightly

packed, ramified (inactive) microglial cells, most probably representing sites of constant microglial residence. Two other layers, at the ILM and among the photoreceptors, were composed of activated microglia. FA-treated eyes showed the same two layers of inactive resident microglia. Within the inner and outer retina, however, striking differences in the numbers of activated microglia were found between the FA-treated eyes and eyes of both control groups. FA treatment was associated with an approximately fourfold decrease in microglial cell counts in the photoreceptor layer and at the ILM. Often, within the photoreceptor layer and at the ILM level of the FA-treated eyes, microscopic field-sized areas with no microglial cells were observed. These findings suggest that synthetic corticosteroid FA inhibited microglial activation and proliferation in the degenerative retinas. We believe that inhibition of microgliosis by FA has a key role in the neuroprotection against photoreceptor cell death.

No ED-1– or ED-2–positive cells were found in the retinas of S334ter rats. We did observe Iba-1–positive, ED-2–negative microglia that did not express the ED-1 marker of phagocytic activity in S334ter rats. These microglia were activated based on their morphology in IBA-1 wholemounts. We observed such cells in RCS rats outside the debris zone. Thus, these cells are phenotypically different from the microglial cells within the debris zone of RCS rats and are similar to microglia found elsewhere in the RCS rat retina. In RCS rats, retinal pigment epithelial cells have lost phagocytic function, leading to the accumulation of shed retinal photoreceptor outer segments and the formation of a large debris zone in the subretinal space. Consequently, microglial cells move to the debris zone to phagocytose the debris. Once activated, they automatically release their toxic molecules, killing the surrounding neurons. In S3343ter rats, microglia become activated but not phagocytic, suggesting that the accelerated photoreceptor cell death we observed in controls occurs independently of significant microglial phagocytosis.

Corticosteroids and Microglia

We have shown in our study that FA treatment was associated with profound quantitative reductions of microglial cells in the degenerative retinas of S334ter-4 rats. The ability of corticosteroids to modulate microglial-mediated neuroinflammation and their neuroprotective effects have been previously described in CNS degenerative diseases.[51–55] In summary, corticosteroids regulate the activity of microglial cells in three ways: synthesis and release of cytotoxic factors and immune signaling.

Inhibition of toxic product synthesis in activated microglia occurs by the influence of steroids on mRNA expression. Cortisol strongly inhibits the microglial expression of inducible nitric oxide synthase (iNOS) mRNA and the production of iNOS, NO, and TNF-α molecules.[56,57] In addition, glucocorticoids stimulate microglial expression of annexin 1 (ANXA 1), a cellular membrane-binding protein that profoundly suppresses the synthesis of COX-2 and iNOS, thus inhibiting the production of proinflammatory cytokines, NO, and prostaglandin E2.[58]

LPS stimulation of microglia causes overexpression of TGF-β1 mRNA.[5] Under normal conditions, TGF-β1 promotes neuronal regeneration, cell adhesion, and elongation of neuronal processes. Overexpression of TGF-β1 maintains the activated microglial state and promotes toxic adhesion of microglia to neurons (see Ref. 5 for review). The synthetic glucocorticoid dexamethasone downregulates microglial gene expression of TGF-β1.[5] Proinflammatory stimulation of microglia triggers signal transduction pathways to stimulate activator protein-1[59]; these pathways start with activation of the enzyme Serine racemase (SRace). Dexamethasone inhibits SRace pro-

moter activity, suppressing SRace mRNA levels.[59] Corticotropin-releasing hormone was shown to exert proapoptotic activity in microglial cells through activation of the caspase-3 pathway and the mitochondrial pathway associated with the generation of ROS by mitochondria and caspase-9 activation.[60]

The immune signaling (antigen-presenting) function of microglial cells may be affected by glucocorticoid interruption of expressions of MHC class I and II[61,62] and interleukins.[62,63] Corticosteroids act upon microglial cells by binding to glucocorticoid receptors (GRs) and mineralocorticoid receptors (MRs). Steroid receptor distribution and activity in microglial cells was shown in detail by Sierra et al.[64] According to their study, microglial cells represent a direct target for steroid hormones because of rich expressions of GRs, MRs, and estrogen receptor alpha. GR was largely detected in the cell membranes and cytosol of microglial processes. It appeared to be the most abundant microglial steroid receptor and was most robustly expressed at both mRNA and protein levels. In addition, they have shown that corticosterone attenuated the production of TNF-α, IL-6, and NO by microglia to levels below the neurotoxic thresholds. Microglial expression of the signaling molecules in response to steroid treatment was out of the scope of this study, although our study confirms microglia-suppressive properties of steroids by showing in vivo that chronic administration of the steroid FA modulates microglial inflammation and preserves ERG and ONL morphology.

Conclusions

We have demonstrated that retinal degeneration in S334ter-4 rats was accompanied by increased numbers of activated microglia in the outer retina and inner retina. We have also demonstrated that low doses of the synthetic corticosteroid FA were neuroprotective in the S334ter-4 model of retinal degeneration. FA treatment was associated with the preservation of retinal electrophysiology, morphology, and suppression of retinal microgliosis. In this study and in the study on RCS rats[33] the lower (0.2 μg/d) FA dose demonstrated better results than did the higher dose. We also observed some degree of ERG and ONL preservation in the fellow (untreated) eyes of the FA 0.2-μg/d–treated group. This finding was not accompanied by microglia depression. The exact nature of this phenomenon is unclear. It might have developed because of systemic distribution of the drug, and it may provide indirect evidence of the higher effectiveness of lower doses.

We used a chronic drug delivery method that we believe is efficacious because of its constant, sustained intraocular drug level. Our findings suggest that the effects of low-dose, sustained-release synthetic corticosteroids, particularly FA, represent a new treatment strategy for retinal degenerations such as RP and possibly other retinal degenerations in human patients.

References

1. Kreutzberg GW. Microglia: a sensor for pathological events in the CNS. *Trends Neurosci.* 1996;19:312–318.
2. Whitton PS. Inflammation as a causative factor in the aetiology of Parkinson's disease. *Br J Pharmacol.* 2007;150:963–976.
3. Kreutzberg GW. Microglia, the first line of defence in brain pathologies. *Arzneimittel-Forschung.* 1995;45:357–360.

4. Nakanishi H. Microglial functions and proteases. *Mol Neurobiol.* 2003;27:163–176.

5. Nichols NR. Glial responses to steroids as markers of brain aging. *J Neurobiol.* 1999;40:585–601.

6. Gehrmann J. Microglia: a sensor to threats in the nervous system? *Res Virol.* 1996;147:79–88.

7. Heneka MT, O'Banion MK. Inflammatory processes in Alzheimer's disease. *J Neuroimmunol.* 2007;184:69–91.

8. Mosley RL, Benner EJ, Kadiu I, et al. Neuroinflammation, oxidative stress and the pathogenesis of Parkinson's disease. *Clin Neurosci Res.* 2006;6:261–281.

9. Tai YF, Pavese N, Gerhard A, et al. Imaging microglial activation in Huntington's disease. *Brain Res Bull.* 2007;72:148–151.

10. Turner MR, Cagnin A, Turkheimer FE, et al. Evidence of widespread cerebral microglial activation in amyotrophic lateral sclerosis: an [11C](R)-PK11195 positron emission tomography study. *Neurobiol Dis.* 2004;15:601–609.

11. Wang J, Gabuzda D. Reconstitution of human immunodeficiency virus-induced neurodegeneration using isolated populations of human neurons, astrocytes, and microglia and neuroprotection mediated by insulin-like growth factors. *J Neurovirol.* 2006;12:472–491.

12. Cuadros MA, Navascues J. The origin and differentiation of microglial cells during development. *Prog Neurobiol.* 1998;56:173–189.

13. Kaur C, Hao AJ, Wu CH, Ling EA. Origin of microglia. *Microsc Res Tech.* 2001;54:2–9.

14. Ling EA, Wong WC. The origin and nature of ramified and amoeboid microglia: a historical review and current concepts. *Glia.* 1993;7:9–18.

15. Herbomel P, Thisse B, Thisse C. Zebrafish early macrophages colonize cephalic mesenchyme and developing brain, retina, and epidermis through a M-CSF receptor-dependent invasive process. *Dev Biol.* 2001;238:274–288.

16. Marin-Teva JL, Calvente R, Cuadros MA, Almendros A, Navascues J. Circumferential migration of ameboid microglia in the margin of the developing quail retina. *Glia.* 1999;27:226–238.

17. Navascues J, Moujahid A, Almendros A, Marin-Teva JL, Cuadros MA. Origin of microglia in the quail retina: central-to-peripheral and vitreal-to-scleral migration of microglial precursors during development. *J Comp Neurol.* 1995;354:209–228.

18. McMenamin PG, Loeffler KU. Cells resembling intraventricular macrophages are present in the subretinal space of human foetal eyes. *Anat Rec.* 1990;227:245–253.

19. Pawate S, Shen Q, Fan F, Bhat NR. Redox regulation of glial inflammatory response to lipopolysaccharide and interferongamma. *J Neurosci Res.* 2004;77:540–551.

20. Orr CF, Rowe DB, Halliday GM. An inflammatory review of Parkinson's disease. *Prog Neurobiol.* 2002;68:325–340.

21. Banati RB, Gehrmann J, Schubert P, Kreutzberg GW. Cytotoxicity of microglia. *Glia.* 1993;7:111–118.

22. Boje KM, Arora PK. Microglial-produced nitric oxide and reactive nitrogen oxides mediate neuronal cell death. *Brain Res.* 1992;587:250–256.

23. Kim SU, de Vellis J. Microglia in health and disease. *J Neurosci Res.* 2005;81:302–313.

24. Aloisi F. Immune function of microglia. *Glia.* 2001;36:165–179.

25. Klegeris A, McGeer PL. Interaction of various intracellular signaling mechanisms involved in mononuclear phagocyte toxicity toward neuronal cells. *J Leukoc Biol.* 2000;67:127–133.

26. Ng TF, Streilein JW. Light-induced migration of retinal microglia into the subretinal space. *Invest Ophthalmol Vis Sci.* 2001;42:3301–3310.

27. Roque RS, Imperial CJ, Caldwell RB. Microglial cells invade the outer retina as photoreceptors degenerate in Royal College of Surgeons rats. *Invest Ophthalmol Vis Sci.* 1996;37:196–203.

28. Zeiss CJ, Johnson EA. Proliferation of microglia, but not photoreceptors, in the outer nuclear layer of the rd-1 mouse. *Invest Ophthalmol Vis Sci.* 2004;45:971–976.

29. Zhang C, Shen JK, Lam TT, et al. Activation of microglia and chemokines in light-induced retinal degeneration. *Mol Vis.* 2005;11:887–895.

30. Roque RS, Rosales AA, Jingjing L, Agarwal N, Al-Ubaidi MR. Retinaderived microglial cells induce photoreceptor cell death in vitro. *Brain Res.* 1999;836:110–119.

31. Srinivasan B, Roque CH, Hempstead BL, Al-Ubaidi MR, Roque RS. Microglia-derived pronerve growth factor promotes photoreceptor cell death via p75 neurotrophin receptor. *J Biol Chem.* 2004;279:41839–41845.

32. Gupta N, Brown KE, Milam AH. Activated microglia in human retinitis pigmentosa, late-onset retinal degeneration, and age-related macular degeneration. *Exp Eye Res.* 2003;76:463–471.

33. Glybina IV, Kennedy A, Ashton P, Abrams GW, Iezzi R. Photoreceptor neuroprotection in RCS rats via low-dose intravitreal sustained-delivery of fluocinolone acetonide. *Invest Ophthalmol Vis Sci.* 2009;50:4847–4857.

34. Thanos S. Sick photoreceptors attract activated microglia from the ganglion cell layer: a model to study the inflammatory cascades in rats with inherited retinal dystrophy. *Brain Res.* 1992;588:21–28.

35. Jaffe GJ, Ben-Nun J, Guo H, Dunn JP, Ashton P. Fluocinolone acetonide sustained drug delivery device to treat severe uveitis. *Ophthalmology.* 2000;107:2024–2033.

36. Jaffe GJ, Martin D, Callanan D, Pearson PA, Levy B, Comstock T. Fluocinolone acetonide implant (Retisert) for noninfectious posterior uveitis: thirty-four-week results of a multicenter randomized clinical study. *Ophthalmology.* 2006;113:1020–1027.

37. Jaffe GJ, Yang CH, Guo H, Denny JP, Lima C, Ashton P. Safety and pharmacokinetics of an intraocular fluocinolone acetonide sustained delivery device. *Invest Ophthalmol Vis Sci.* 2000;41:3569–3575.

38. D'Cruz PM, Yasumura D, Weir J, et al. Mutation of the receptor tyrosine kinase gene Mertk in the retinal dystrophic RCS rat. *Hum Mol Genet.* 2000;9:645–651.

39. Nandrot E, Dufour EM, Provost AC, et al. Homozygous deletion in the coding sequence of the c-mer gene in RCS rats unravels general mechanisms of physiological cell adhesion and apoptosis. *Neurobiol Dis.* 2000;7:586–599.

40. LaVail MM, Yasumura D, Matthes MT, et al. Ribozyme rescue of photoreceptor cells in P23H transgenic rats: long-term survival and late-stage therapy. *Proc Natl Acad Sci U S A.* 2000;97:11488–11493.

41. Matthes MT, LaVail MM. Inherited retinal dystrophy in the RCS rat: composition of the outer segment debris zone. *Prog Clin Biol Res.* 1989;314:315–330.

42. Porrello K, LaVail MM. Immunocytochemical localization of chondroitin sulfates in the interphotoreceptor matrix of the normal and dystrophic rat retina. *Curr Eye Res.* 1986;5:981–993.

43. Imai Y, Ibata I, Ito D, Ohsawa K, Kohsaka S. A novel gene iba1 in the major histocompatibility complex class III region encoding an EF hand protein expressed in a monocytic lineage. *Biochem Biophys Res Commun.* 1996;224:855–862.

44. Dijkstra CD, Dopp EA, Joling P, Kraal G. The heterogeneity of mononuclear phagocytes in lymphoid organs: distinct macrophage subpopulations in the rat recognized by monoclonal antibodies ED1, ED2 and ED3. *Immunology.* 1985;54:589–599.

45. Grondahl J, Riise R, Heiberg A, Leren T, Christoffersen T, Bragadottir R. Autosomal dominant retinitis pigmentosa in Norway: a 20-year clinical follow-up study with molecular genetic analysis. Two novel rhodopsin mutations: 1003delG and I179F. *Acta Ophthalmol Scand.* 2007;85:287–297.

46. Zhang XL, Liu M, Meng XH, et al. Mutational analysis of the rhodopsin gene in Chinese ADRP families by conformation sensitive gel electrophoresis. *Life Sci.* 2006;78:1494–1498.

47. Green ES, Menz MD, LaVail MM, Flannery JG. Characterization of rhodopsin mis-sorting and constitutive activation in a transgenic rat model of retinitis pigmentosa. *Invest Ophthalmol Vis Sci.* 2000;41:1546–1553.

48. Lee D, Geller S, Walsh N, et al. Photoreceptor degeneration in Pro23His and S334ter transgenic rats. *Adv Exp Med Biol.* 2003;533:297–302.

49. Liu C, Li Y, Peng M, Laties AM, Wen R. Activation of caspase-3 in the retina of transgenic rats with the rhodopsin mutation s334ter during photoreceptor degeneration. *J Neurosci.* 1999;19:4778–4785.

50. Song Y, Zhao L, Tao W, Laties AM, Luo Z, Wen R. Photoreceptor protection by cardiotrophin-1 in transgenic rats with the rhodopsin mutation s334ter. *Invest Ophthalmol Vis Sci.* 2003;44:4069–4075.

51. Dhawan N, Puangco J, Jandial R. In search of a treatment for Alzheimer's disease and potential immunonosuppresive therapeutic interventions. *Neuro Endocrinol Lett.* 2008;29:410–420.

52. Dheen ST, Kaur C, Ling EA. Microglial activation and its implications in the brain diseases. *Curr Med Chem.* 2007;14:1189–1197.

53. Reichardt HM, Gold R, Luhder F. Glucocorticoids in multiple sclerosis and experimental autoimmune encephalomyelitis. *Exp Rev Neurotherapeut.* 2006;6:1657–1670.

54. Schroter A, Lustenberger RM, Obermair FJ, Thallmair M. High-dose corticosteroids after spinal cord injury reduce neural progenitor cell proliferation. *Neuroscience.* 2009;161:753–763.

55. Viscomi MT, Florenzano F, Latini L, Amantea D, Bernardi G, Molinari M. Methylprednisolone treatment delays remote cell death after focal brain lesion. *Neuroscience.* 2008;154:1267–1282.

56. Drew PD, Chavis JA. Inhibition of microglial cell activation by cortisol. *Brain Res Bull.* 2000;52:391–396.

57. Golde S, Coles A, Lindquist JA, Compston A. Decreased iNOS synthesis mediates dexamethasone-induced protection of neurons from inflammatory injury in vitro. *Eur J Neurosci.* 2003;18:2527–2537.

58. Parente L, Solito E. Annexin 1: more than an anti-phospholipase protein. *Inflamm Res.* 2004;53:125–132.

59. Wu S, Barger SW. Induction of serine racemase by inflammatory stimuli is dependent on AP-1. *Ann N Y Acad Sci.* 2004;1035:133–146.

60. Ock J, Lee H, Kim S, et al. Induction of microglial apoptosis by corticotropin-releasing hormone. *J Neurochem.* 2006;98:962–972.

61. Kiefer R, Kreutzberg GW. Effects of dexamethasone on microglial activation in vivo: selective downregulation of major histocompatibility complex class II expression in regenerating facial nucleus. *J Neuroimmunol.* 1991;34:99–108.

62. Li M, Wang Y, Guo R, Bai Y, Yu Z. Glucocorticoids impair microglia ability to induce T cell proliferation and Th1 polarization. *Immunol Lett.* 2007;109:129–137.

63. Snyder DS, Unanue ER. Corticosteroids inhibit murine macrophage Ia expression and interleukin 1 production. *J Immunol.* 1982;129:1803–1805.

64. Sierra A, Gottfried-Blackmore A, Milner TA, McEwen BS, Bulloch K. Steroid hormone receptor expression and function in microglia. *Glia.* 2008;56:659–674.